Farfield Ion Current Density Measurements before and after the NASA HiVHAc EDU2 Vibration Test

Wensheng Huang*, Hani Kamhawi†, and Rohit Shastry‡
National Aeronautics and Space Administration Glenn Research Center, Cleveland, Ohio, 44135

There is an increasing need to characterize the plasma plume of the NASA HiVHAc thruster in order to better understand the plasma physics and to obtain data for spacecraft interaction studies. To address this need, the HiVHAc research team is in the process of developing a number of plume diagnostic systems. This paper presents the initial results of the farfield current density probe diagnostic system. Farfield current density measurements were carried out before and after a vibration test of the HiVHAc engineering development unit 2 that simulate typical launch conditions. The main purposes of the current density measurements were to evaluate the thruster plume divergence and to investigate any changes in the plasma plume that may occur as a result of the vibration test. Radial sweeps, as opposed to the traditional polar sweeps, were performed during these tests. The charged-weighted divergence angles were found to vary from 16 to 28 degrees. Charge density profiles measured pre- and post-vibration-test were found to be in excellent agreement. This result, alongside thrust measurements reported in a companion paper, confirm that the operation of the HiVHAc engineering development unit 2 were not altered by full-level/random vibration testing.

I. Introduction

THE development of the NASA High Voltage Hall Accelerator (HiVHAc) continues to progress steadily. This project is funded by the NASA Science Mission Directorate's (SMD's) In-Space Propulsion Technology Project (ISPT) to deliver a Hall thruster beyond the current state-of-the-art (SotA) that is capable of closing various Discovery class missions. Recent mission studies in 2009 showed that the 3.5-kW HiVHAc is able to outperform a SotA 4.5-kW flight Hall thruster by delivering 6-12% more mass on four missions of interest.[1] These missions include Vesta-Ceres rendezvous (the Dawn mission), Koppf comet rendezvous, Nereus (a near-Earth asteroid) sample return, and NEARER, which involves two near-Earth asteroid returns. The thrust profiles of the missions range from ones that favor high specific impulse to ones that favor high thrust-to-power demonstrating the wide throttle-ability of the 3.5-kW HiVHAc.

The current iteration of the HiVHAc Hall thruster is the Engineering Development Unit 2 (EDU2), which was previously called engineering model-reworked (EM-R). Its predecessor is the Engineering Development Unit 1 (EDU1), which was previously called the engineering model (EM). Like the EDU1, the EDU2 features a discharge channel replacement mechanism designed to guarantee long operational life time for high specific impulse (high discharge voltage) operation. Improvements in the design of the EDU2 over the EDU1 include better thermal management, simpler design for the life-extending channel replacement mechanism, and superior voltage isolation. The EDU2 has undergone the performance acceptance test (PAT) and the vibration test.[2] To check that the vibration test did not negatively impact the operation of the thruster, thrust and ion current density measurements were taken before and after the vibration test. The performance characterization of the EDU2 is concurrently published in a separate paper.[3] The ion current density measurements are described in this paper.

In the past, HiVHAc-related research had been focused on increasing overall performance and life time. Recently, the research team determined that there is a need to characterize the behavior of the plume. Characterization of the plasma plume will benefit the development of the HiVHAc by providing valuable insights into the behavior of the thruster as well as aid in the evaluation of lifetime and studies of spacecraft-plume interactions. Of particular interest to the research team are the various physical phenomena that contribute to the

* Research Engineer, Propulsion and Propellants, wensheng.huang@nasa.gov, AIAA Member.
† Research Engineer, Propulsion and Propellants, hani.kamhawi-1@nasa.gov, AIAA Associate Fellow.
‡ Research Engineer, Propulsion and Propellants, rohit.shastry@nasa.gov, AIAA Member.

overall efficiency including plume divergence, current utilization, mass utilization, multiply-charged species fraction, and ion energy distribution functions.

Currently, the research team has identified two spatial regions of interest. Characterization of the near-field (<1 nominal thruster diameter) is of great importance to understanding the erosion behavior of the discharge channel. Information of interest in this region includes plasma potential, plasma density, electron temperature, and energy distribution functions. The primary diagnostics currently in consideration for this region include near-field Langmuir probe, near-field Faraday probe, and emissive probe. Characterization of the far-field (>5 mean thruster diameters) is of great importance to performance and plume interaction studies. Information of interest in this region includes plasma density, electron temperature, ion current density, multiply-charged species fraction, and ion energy distribution function. The primary diagnostics currently in consideration for this region include far-field Langmuir probe, far-field Faraday probe, ExB probe, and retarding potential analyzer (RPA). Development of these probes and accompanying systems are currently in progress and only farfield Faraday probe data is available as of the writing of this paper.

This paper will describe farfield ion current density measurements obtained during a series of tests associated with the vibration testing of the HiVHAc EDU2. The purpose of the vibration test is to simulate the mechanical conditions that the thruster will experience on a typical launch to orbit. One set of current density measurements was made shortly before the vibration test and another set was made after the vibration test. The first purpose of the current density measurements was to determine the plume divergence of the thruster. The second purpose was to determine whether the plume profile and divergence angle change when the thruster undergoes vibration testing. These measurements provide an extra metric (in addition to thrust measurements) for determining how well the design of the EDU2 copes with the vibrational environment of a typical launch. Should the thrust change after vibration testing, the ion current density measurements would be of great help in determining the root cause.

For the tests described in this paper, a farfield Faraday probe was used to measure ion current density as a function of radial position, as opposed to the more traditional approach of measuring as a function of polar position. This was done primarily due to equipment constraint but also to study the effectiveness of radial sweeps versus polar sweeps. Polar sweeps will be performed for comparison purposes at a future date.

Brown's works provide excellent overviews of the use of farfield polarly-swept Faraday probe in a Hall thruster environment.[4, 5] Radially-swept Faraday probe measurements are often used in ion thruster studies. Several papers by NASA ion thruster researchers provide excellent overviews of how radially-swept ion current density measurements are carried out for ion thrusters.[6, 7] Another paper by the Aerospace Corporation research team describes how polar sweeps can be carried out for an ion thruster.[8]

II. Experimental Setup

A. Thruster and Test Matrix

The NASA High Voltage Hall Accelerator (HiVHAc) Engineering Development Unit 2 (EDU2) is a 3.9-kW high-voltage Hall thruster. The propellant is xenon. For the ion current density tests, the discharge voltage is varied from 200 to 650 V and the discharge current is varied from 1.25 to 7.92 A. The corresponding discharge power ranged from 300 to 3900 W. Magnetic field settings are selected to optimize performance. Cathode mass flow rate is fixed at 0.45 mg/s. A keeper current of 1.00 A is applied. Anode efficiency ranged from about 20% at low discharge power to 65% at nominal discharge power. A total of 35 conditions were tested during the pre-vibration-test study. Due to time constraint, only 5 of those conditions were selected for the post-vibration-test study. Figure 1 shows a picture of the NASA HiVHAc EDU2.

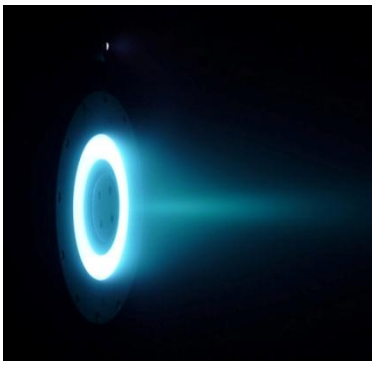

Figure 1. NASA HiVHAc EDU2 in operation.

B. Vacuum Facility and Motion Stages

All ion current density measurements were taken in vacuum facility 12 (VF12) at the NASA Glenn Research Center (GRC). This facility is equipped with eight cryo-panels with a total pumping speed of 1,000,000 L/s on air. VF12 is a cylindrical vacuum chamber measuring 9 m in length and 3 m in diameter. The chamber is roughly divided into two halves. The half of the chamber away from the end-cap is called the cryo section, and is occupied by the cryo-panels and associated structures. The half of the chamber next to the end-cap is called the thruster section. The thruster fires from a position close to the end-cap in the thruster section along the centerline of the chamber towards the cryo-panels. There is a graphite beam dump located halfway into the chamber to prevent direct impingement of the beam on the cryo-panels. With the exception of a few access ports and the motion stages, the entire thruster section is covered by graphite panels to reduce back sputtered material. Background pressure was monitored via two nude ion gauges. For reference, the average of the gauge pressure readings is 5.9e-6 Torr when the anode mass flow rate is 2.1 mg/s, and 1.4e-5 Torr when the anode mass flow rate is 7.7 mg/s. Cathode mass flow rate is fixed at 0.45 mg/s. Pressure readings given here have been corrected for xenon.

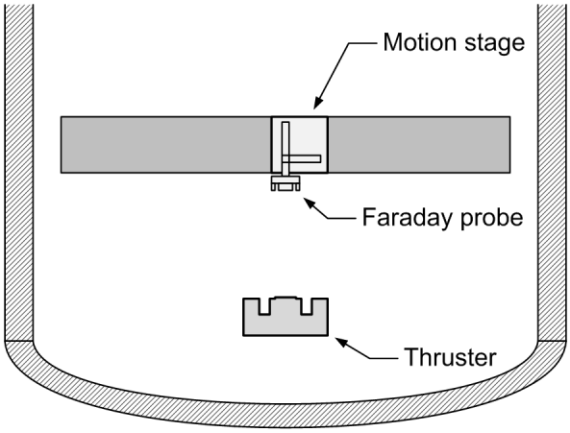

Figure 2. Mechanical setup for the experiment.

Figure 2 shows a diagram of the mechanical setup for the two ion current density tests. Due to ongoing upgrades to the diagnostics systems in VF12, two different motion stages were used for the ion current density tests. Care was taken to make sure the Faraday probe was aligned in the same fashion regardless of which motion stage was in use. For both tests, the Faraday probe is scanned radially, in the horizontal plane that bisects the thruster body, at 5 mean thruster diameters away from the channel exit plane. The cathode was located out of plane at the 12 o'clock position when viewing the thruster face-on. Mean thruster diameter is defined as the average of the inner and outer boron nitride channel wall diameters. This value will be used to normalize the spatial coordinate of the ion current density tests and will be abbreviated as MTD. Channel exit plane is defined as the axial location where the boron nitride channel wall meets the front surface of the boron nitride channel and is the same for both inner and outer channel walls. During the pre-vibration ion current density test, the radial stage used had a travel of ~11 MTD, while during the post-vibration test, the radial stage used had a travel of ~16 MTD. For both tests, the positioning system has a relative uncertainty of ±0.05 mm and an absolute uncertainty of ±2 mm.

C. Faraday Probe

The Faraday probe design used in both ion current density tests is based on a design previously used at the Glenn Research Center. The new design contains a modification based on experiences obtained from another ion current density test that took place before the pre-vibration-test ion current density test. Section VI contains a more detailed description of why the modification was made. Figure 3 shows a diagram of the Faraday probe used for the two ion current density tests that are described in this paper. The collector area is a circle of diameter 17.39 ± 0.02 mm. The overall probe is roughly 28 mm in diameter. The collector and guard ring are made of molybdenum (to minimize secondary electron emission) and the back is made of macor.

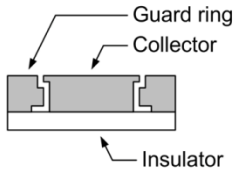

Figure 3. Faraday probe design.

D. Data Acquisition

The data taking process is automated in a LabVIEW program on a dedicated data acquisition (DAQ) computer that is connected to the various test equipments. The motion stage is controlled by an Aerotech Ensemble CP20 motion controller, which receives motion commands from the DAQ computer. The signal from the Faraday probe is connected to a Faraday probe circuit box, which includes calibrated current shunts and isolation amplifiers. The Faraday probe is biased to -20 V with respect to ground via a power supply connected to the circuit box. This bias voltage is chosen based on traces taken at several bias voltages. The isolated signals from the circuit box are fed into an NI USB-6351 data acquisition device, which is commanded by the DAQ computer. Figure 4 shows the electronic setup for the two ion current density tests.

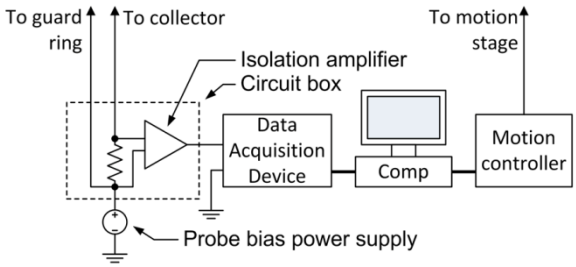

Figure 4. Electronic setup for the experiment.

III. Data Reduction

A. Charge-Weighted Divergence Equation for Radial Sweep

The cosine of the momentum-weighted divergence angle in Hall thruster testing is also called the "thrust correction factor for beam divergence" in ion thruster testing.[6] This angle characterizes the decrease in thrust due to propellant particles that have radial velocity components. Due to difficulties in measuring momentum-weighted divergence angle, it is common practice in the Hall thruster community to measure the charge-weighted divergence angle instead. If the plume is axisymmetric, the charge-state ratios are constant, and the average particle velocity is constant throughout the measurement domain then the aforementioned angles are equal.[5] Equation (1) can be used to derive charge-weighted divergence angle from polarly-swept ion current density measurement.

$$< \cos\delta >_j = \frac{2\pi R^2 \int_0^{\pi/2} j(\theta)\cos\theta\sin\theta\, d\theta}{2\pi R^2 \int_0^{\pi/2} j(\theta)\sin\theta\, d\theta} \tag{1}$$

In this equation, δ is the charged-weighted divergence angle, R is the distance from the probe to the thruster, which is approximated as a point source, $j(\theta)$ is the ion current density measured with the Faraday probe facing the thruster as a function of the polar angle θ. The standard range of integration is from 0° to 90° with respect to the thruster firing axis. For a radially-swept probe where the surface normal vector of the collection area is always pointed along the thruster firing axis, the measured current density is the axial component of the local ion current density. For such a probe, Eq. (1) can be modified into Eq. (2) to calculate the charge-weighted divergence angle.

$$< \cos\delta >_j = \frac{2\pi \int_0^{\infty} j_z(r)\cos\theta\, r\, dr}{2\pi \int_0^{\infty} j_z(r)\, r\, dr},\ \cos\theta = \frac{z_p}{\sqrt{r^2 + z_p{}^2}} \tag{2}$$

In this equation, $j_z(r)$ is the axial ion current density as a function of the radial coordinate r. z_p is the axial distance from the probe to the thruster and is constant for a radial sweep. To replicate the same limits of integration as the polar sweeps, the limits must range from 0 to ∞, which is not practical. The next section will discuss some possible limits of integration that can be used with a farfield radially-swept Faraday probe.

B. Limits of Integration

Choosing the limits of integration for radially-swept ion current density data is less straightforward than for polarly-swept ion current density data. Unlike a polar sweep, a radial sweep can never encompass the entire plume that have a downstream-pointing axial velocity component. This is because it is physically impossible to extend the measurement domain out to infinity. As it turns out, there are also good reasons not to extend the limits of integration to infinity. Although most of the ions coming from the thruster are beam ions, there will always be non-beam ions in the measurement domain, as well as background noise in the environment and the electrical circuit.

There are at least two major sources of non-beam ions, charge exchange events and the cathode plasma. Unlike beam ions, these non-beam ions radiate out almost isotropically and will dominate the measurement signal at high polar angles. Here, polar angle is defined as 0° for ions traveling purely axially and 90° for ions traveling purely radially. Furthermore, it is not possible to completely eliminate noise and offsets in the measurement signal. These undesirable additions to the signal is less prominent in polar traces because the probe is at a fixed distance from the thruster, which will mean a fixed non-beam ion signal if the non-beam sources are isotropic, and because the finite sweep range limits the influence of background noise and offsets. For a radial sweep, there will come a point when the signal is dominated by aforementioned undesirable effects. If the limits of integration are set too large, the non-beam ions and noise will typically cause one to overestimate the divergence angle. If the limits of integration are set too small, one may not capture enough beam ions and will underestimate the divergence angle.

Data analysis was initially performed with two types of integration limits, fixed limits and threshold-based limits. For the fixed-limits approach, the data is integrated from 0° to -45°, where the negative sign indicates that the end angle is in the 3 o'clock direction when viewing the thruster face-on. This approach did not produce desirable results because the 45° boundary sometimes capture too many non-beam ions and sometimes capture too few beam ions. The ratio of total beam current to discharge current calculated by this approach reached as high as 0.99. This was deemed unlikely to be real based on values typically found in Hall thruster testing.

The threshold-based limits yield more reasonable total beam current to discharge current ratio, which reached up to only 0.83 for these limits. In the threshold-based-limits approach, the limits are established based on the two points at which the current density reaches a certain percentage of the peak current density. Borrowing from laser beam physics, the threshold levels are established based on multiples of e^{-1}. (The wings of typical Faraday probe traces resemble a Gaussian distribution.). Several threshold values were tried and the e^{-3} and e^{-4} values were chosen for data presented in this paper. These threshold levels are labeled as "3-e" and "4-e", and the threshold value are equal to 5% and 1.8%, respectively. Figure 5 shows a typical radially-swept Faraday probe trace along with the corresponding integration limits for the 3-e and 4-e approaches.

Over the course of this study, it was determined that there was insufficient data to calculate the right value for the limits of integration. Instead, both 3-e and 4-e limits were applied for purpose of comparing pre-vibration data to post-vibration data. Then, both limits were applied for efficiency analysis and the one that presents a more reasonable answer is shown in this paper.

C. Efficiency Model

The efficiency model that will be used for this paper was developed and successfully used in many recent Hall thruster performance studies.[5, 9, 10] This model, shown in Eq. (3), breaks the physical effects that contribute to the anode efficiency (does not account for cathode and magnet) of a Hall thruster into five factors.

$$\eta_a = \frac{T^2}{2\dot{m}_a P_d} = \eta_q \eta_v \eta_d \eta_b \eta_m \tag{3}$$

In this equation, T is the thrust, $\dot{m}_a$ is the anode mass flow rate, P_d is the discharge power, η_q is the charge utilization efficiency, η_v is the voltage utilization efficiency, η_d is the plume divergence efficiency, η_b is the current utilization efficiency, and η_m is the mass utilization efficiency. Traditionally, the charge and voltage utilization efficiencies are measured using ExB probe and RPA, respectively. Since neither measurement is available as of the writing of this paper, some of the five efficiency factors cannot be calculated. However, we would like to have some form of sanity check on how well chosen our integration limits are. By making assumptions based on past Hall thruster experiments and modifying the phenomenological efficiency model, we can calculate an approximate anode efficiency using only the ion current density measurements available.

We will now look at each of the five efficiency factor and attempt to make reasonable approximations where data is not available. It is difficult to estimate the charge utilization efficiency without ExB measurements. However, past ExB tests performed on state-of-the-art Hall thruster has shown that this value typically varies from 0.97 to 0.99 and

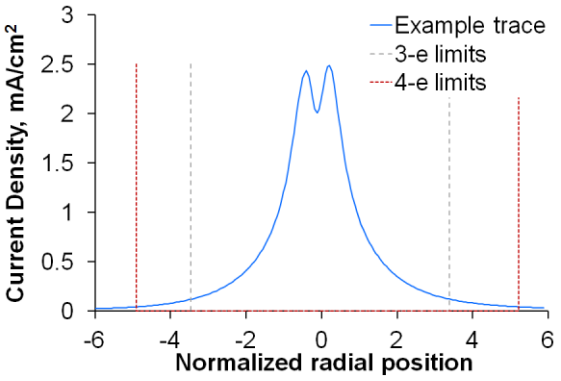

Figure 5. Example radially-swept Faraday probe trace and integration limits.

will be assumed to equal to 1 for the present analysis.[11] Equation (4) shows the original form of the voltage utilization efficiency.

$$\eta_v = 1 - \frac{V_L}{V_d} \tag{4}$$

In this equation, V_L is the loss voltage, which characterizes the average amount of the discharge voltage V_d that is not experienced by the ions. The two main causes for the presence of loss voltage are the overlap between the ionization and acceleration zones and the coupling voltage needed to extract electrons from the cathode. For the purpose of calculating the voltage utilization efficiency, the loss voltage is assumed to be ~15 V based on measurement from another state-of-the-art Hall thruster of comparable power level.[10] Equation (5) shows the relationship between the plume divergence efficiency and charge-weighted divergence angle.

$$\eta_d = (<\cos\delta>_j)^2 \tag{5}$$

The charge-weighted divergence angle is calculated from the farfield Faraday probe data. The total ion current can be calculated using the denominator in Eq. (1) or (2). The total ion current can then be used to calculate the current utilization efficiency.[5] This utilization factor is an indicator of the amount of discharge power that is fed to thrust-producing ions as oppose to non-thrust-producing electrons. Equation (6) shows the relationship between the total ion current and the current utilization efficiency.

$$\eta_b = \frac{I_b}{I_d} \tag{6}$$

In this equation, I_b is the total ion current and I_d is the discharge current. Lastly, Eq. (7) shows how the mass utilization efficiency is typically calculated when charge-state information is available. The mass utilization is a fraction of the total beam-ion mass flux generated by the thruster over the mass flux supplied to the thruster anode.

$$\eta_m = \xi\eta_b \sum_i \frac{\Omega_i}{Z_i},\ \xi = \frac{M_{xe} I_d}{\dot{m}_a e} \tag{7}$$

In this equation, ξ is the exchange ratio, Ω_i is the ion current fraction of the i-th species, Z_i is the charge state of the i-th species, M_{xe} is the mass of a xenon atom, I_d is the discharge current, and e is the fundamental charge constant. In the absence of charge-state information, it is still possible to estimate the beam-ion mass flux by ignoring the multiply-charged correction in Eq. (7). However, doing so can give rise to mass utilization efficiency of greater than 1 as the multiply-charged ions will show up as multiple singly-charged ions in such a calculation. To avoid this potential issue, we will use the measured thrust to estimate the mass utilization. Although using the measured thrust defeats one of the original purpose of the phenomenological model (which is to provide a check on the thrust-derived anode efficiency), it will give us a more realistic check on how well we have chosen our integration limits. Equation (8) shows how the mass utilization efficiency is estimated from the measured thrust.

$$\eta_m = \frac{T}{\dot{m}_a <v_i>},\ <v_i> \approx \sqrt{\frac{2e(V_d - V_L)}{M_{xe}}} \tag{8}$$

In this equation, $<v_i>$ is the average ion velocity, which is calculated by assuming that singly-charged ions undergo a total electrical potential drop equal to the discharge voltage minus the loss voltage. The loss voltage is assumed to be ~15 V. We can now compute the anode efficiency using a combination of ion current density and thrust, and compare the value to anode efficiency derived from only thrust measurement in order to check the validity of the integration limits. To clarify the terminology for the remainder of this paper, we will call the anode efficiency derived from only measured thrust "thrust-derived anode efficiency", and we will call the anode efficiency derived from the aforementioned 5-factor phenomenological model "5-factor anode efficiency".

D. Uncertainty Analysis

There are two main sources of uncertainty for the ion current density measurements. First, uncertainty in the current density can be up to ±0.1 mA/cm^2 due to instrumentation drift as characterized by pre-test and post-test calibrations, though typical value is closer to ±0.01 mA/cm^2. Second, the effective collection area (expanded due to ions hitting the collector from the side) was difficult to characterize. Investigations performed by Brown suggest that if collector and guard ring have similar side wall areas, the maximum effective collection area is equal to the area of the collector front surface plus one half of the gap area when the probe is viewed face-on.[5] This would suggest that the real collection area can be as much as 6% greater than the area of the collector front surface. Brown also suggested a correction factor to remove this source of uncertainty for a polarly-swept probe. Due to difficulties in characterizing the effective collection area, the aforementioned correction factor was not applied and the increase in uncertainty is noted. An explanation of the difficulties involved in characterizing the effective collection area for a radially-swept probe is given in a later section. The combination of these two effects puts the typical uncertainty on ion current density at ±0.01 mA/cm^2, or +0%/-6%, whichever is greater in magnitude.

The uncertainty in the divergence angle is somewhat difficult to quantify and is only meaningful when taken together with the choice of integration limits. As will be seen, changing the integration limit from 3-e to 4-e typically increases the calculated divergence angle by 3-4°. Since finding the right integration limit is one of the goals of this paper, the associated uncertainty is left unanalyzed for the time being. We plan to study this topic again after obtaining polarly-swept Faraday probe data.

IV. Results

A. Ion Current Density Profile

Figures 6-10 show comparisons of the ion current density profiles measured before and after the vibration test. The profile measured before the vibration test is labeled "Pre-vib" and the profile measured after is labeled "Post-vib" in the legend of each figure. For each figure, the radial position is normalized by the mean thruster diameter and is equal to zero along the centerline of the thruster.

From figs. 6-10, we can see a fairly good match between the pre-vibration-test data and the post-vibration-test data. Generally, the two sets of data have the same shape except at the very center of the plume. Variations in the center of the ion density profile have been previously observed during the performance acceptance test. Interestingly, unpublished Faraday probe data on another SotA Hall thruster of comparable power in a much bigger chamber with near identical setup shows far less variations in the centers of the profiles. We hypothesize that the size of the chamber and the surface condition of the chamber wall may have been influencing how the plasma couples to the chamber and the exact shape of the current density profile. Although the centers of the plume profiles differ, the magnitudes of the current densities match well.

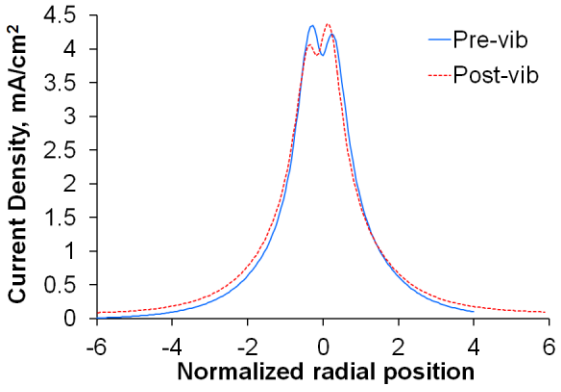

Figure 6. Ion current density profile comparison for operation at 300 V and 1 kW.

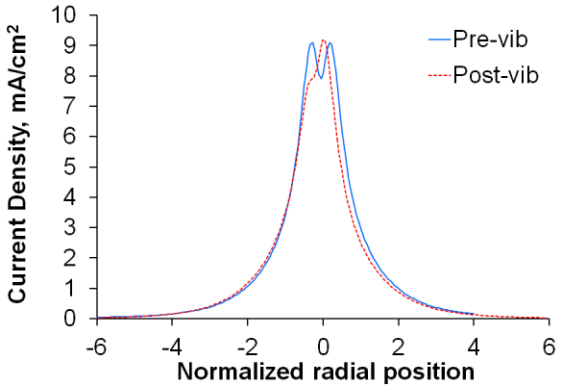

Figure 7. Ion current density profile comparison for operation at 400 V and 2 kW.

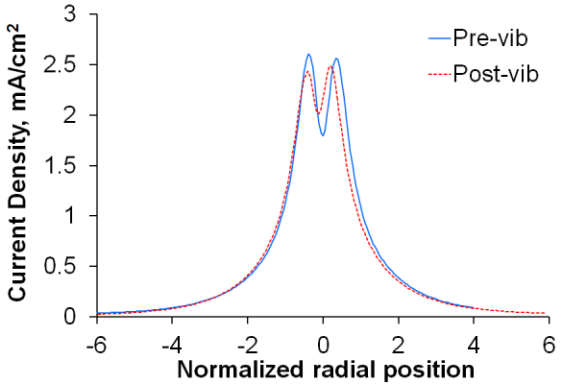

Figure 8. Ion current density profile comparison for operation at 500 V and 1 kW.

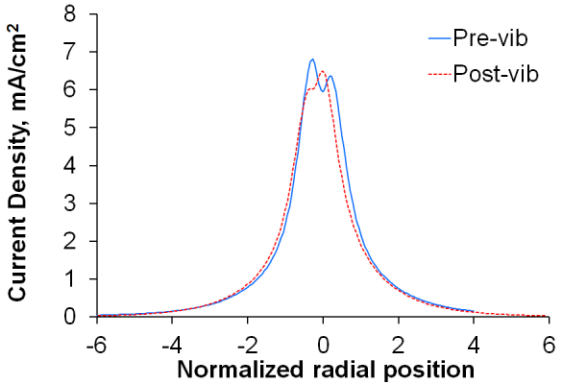

Figure 9. Ion current density profile comparison for operation at 500 V and 2 kW.

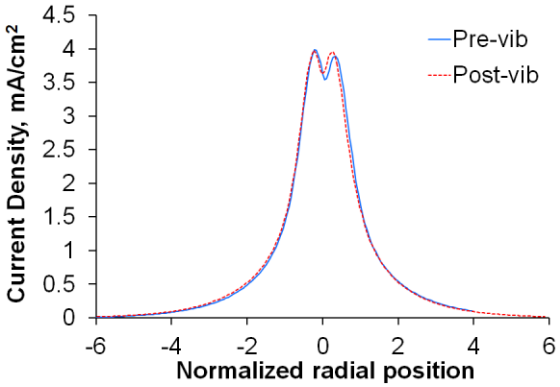

Figure 10. Ion current density profile comparison for operation at 650 V and 2 kW.

B. Divergence Angle, Total Ion Current, and Efficiency Analysis

Table 1 shows a comparison of the divergence angle and total ion current for pre-vibration and post-vibration ion current density measurements. Analysis was carried out using both 3-e and 4-e integration limits. The analysis show

Table 1. Comparison of divergence angle and total ion current between pre-vibration and post-vibration ion current density measurements. *Pre-vibration measurements are labeled as "Pre-vib" and Post-vibration measurements are labeled as "Post-vib".*

				Divergence angle, °		Total Ion Current, A (±10%)	
Time	Discharge voltage, V (±0.5V)	Discharge current, A (±0.5%)	Discharge power, W (±0.5%)	3-e limits (cut off at 5% of peak)	4-e limits (cut off at 1.8% of peak)	3-e limits (cut off at 5% of peak)	4-e limits (cut off at 1.8% of peak)
Pre-vib	300	3.34	1001	18.0	21.0	2.08	2.36
	400	5.03	2013	16.0	19.1	3.16	3.66
	500	2.04	1019	18.8	23.6	1.30	1.57
	500	4.07	2037	16.8	20.2	2.55	2.97
	650	3.05	1982	17.4	20.8	1.77	2.05
Post-vib	300	3.33	999	17.5	20.2	2.07	2.33
	400	4.97	1988	15.9	19.3	3.38	3.94
	500	2.00	1000	18.9	24.0	1.36	1.68
	500	3.95	1975	16.6	20.3	2.59	3.06
	650	3.07	1996	16.8	20.2	1.74	1.99

that the divergence angles for pre-vibration and post-vibration data are matching to within less than 1° and the total ion current to within 8%. These numbers combined with the current density profile suggests that the plasma plume is largely unchanged between pre-vibration test and post-vibration test. At first glance, it may seem strange that the divergence angles match so well even though the signals at the center of the ion current density profiles are not in perfect agreement. The reason for this is expressed in the integrals in Eq. (1) and (2). The area element associated with ion current measured at the center is much smaller than the area element associated with off-center data. As a result, the part of the ion current density profile with the highest intensity also has the lowest weight in determining the divergence angle of the thruster.

Table 2 shows the efficiency analysis for the pre-vibration ion current density measurements. Included in this table are the measured thrust and the thrust-derived anode efficiency. Details on how the thrust measurements were made can be found in a companion paper.[3] Also shown are the divergence angle, total ion current, plume divergence efficiency, and current utilization efficiency derived using the 4-e integration limit. Lastly, the modified phenomenological model is used to calculate the other three of the five efficiency factors, and the result is combined with the Faraday-probe-derived information to obtain an independent 5-factor-based anode efficiency. Only the end result of this calculation is shown in Table 2. A separate calculation, not shown in the table, showed that the 5-factor anode efficiency derived using 3-e limits was, on the average, 4.8% too low compared to the thrust-derived anode efficiency. In contrast, results from calculations made using the 4-e limits was, on the average, within 1% of the thrust-only anode efficiency. This is the rationale for presenting only 4-e data in Table 2. Within Table 2, thrust-derived anode efficiency is highlighted in blue, 5-factor anode efficiency is highlighted in green, and the difference between the two (thrust-derived minus 5-factor) is highlighted in red. Averaging the entire last column yield -0.7%, which shows that the 4-e integration limits give reasonable results.

No efficiency analysis was carried out with the post-vibration test data as Table 1 already show the post-vibration test data match the pre-vibration test data very well.

Table 2. Efficiency analysis for pre-vibration ion current density and thrust data.

Disch. voltage, V (±0.5V)	Disch. current, A (±0.5%)	Disch. power, W (±0.5%)	Thrust, mN	Thrust-derived anode efficiency	Divergence angle, °	Total ion current, A	Plume divergence efficiency	Current utilization	5-factor anode efficiency	Difference (Thrust-derived minus 5-factor)
200	1.51	302	16	19%	22.4	0.78	85%	52%	20%	-0.4%
200	2.50	500	30	29%	23.4	1.35	84%	54%	26%	3.5%
200	4.98	996	63	34%	22.2	3.17	86%	64%	34%	0.3%
200	7.55	1510	99	40%	20.9	5.07	87%	67%	40%	-0.5%
300	1.70	510	27	32%	20.2	1.06	88%	62%	32%	0.4%
300	3.33	999	60	46%	20.2	2.33	88%	70%	44%	1.8%
300	4.98	1494	90	48%	19.7	3.61	89%	72%	48%	0.2%
300	6.65	1995	119	49%	19.0	4.91	89%	74%	51%	-1.7%
400	1.25	500	22	30%	28.1	1.12	78%	90%	40%	-9.9%
400	2.51	1004	58	54%	20.9	2.03	87%	81%	54%	-0.7%
400	3.76	1504	84	54%	19.8	2.98	89%	79%	55%	-1.3%
400	4.97	1988	110	54%	19.3	3.94	89%	79%	57%	-2.6%
400	6.27	2508	138	56%	19.1	4.91	89%	78%	58%	-2.1%
400	7.41	2964	162	56%	18.9	5.74	90%	78%	59%	-2.4%
500	2.00	1000	52	58%	24.0	1.68	83%	84%	59%	-0.4%
500	2.96	1480	75	54%	20.7	2.46	88%	83%	58%	-3.4%
500	3.95	1975	93	53%	20.3	3.06	88%	77%	56%	-3.0%
500	5.00	2500	119	54%	19.0	3.96	89%	79%	60%	-5.1%
500	6.01	3005	142	55%	18.5	4.73	90%	79%	61%	-5.5%
500	7.02	3510	165	56%	18.1	5.44	90%	78%	61%	-4.8%
500	7.90	3950	189	59%	17.8	6.06	91%	77%	63%	-4.4%
600	1.67	1002	38	40%	19.9	0.92	88%	55%	37%	2.1%
600	2.56	1536	62	46%	19.8	1.68	89%	66%	46%	0.9%
600	3.37	2022	81	49%	20.6	2.19	88%	65%	47%	2.1%
600	4.19	2514	109	58%	19.9	2.95	88%	70%	55%	2.3%
600	5.02	3012	136	61%	18.5	3.66	90%	73%	59%	1.9%
600	5.85	3510	160	62%	16.6	4.34	92%	74%	62%	-0.7%
600	6.48	3888	179	63%	16.5	4.90	92%	76%	65%	-1.3%
650	1.54	1001	37	42%	20.0	0.76	88%	49%	32%	9.1%
650	2.24	1456	58	50%	19.7	1.40	89%	63%	49%	0.8%
650	3.07	1996	82	55%	20.2	1.99	88%	65%	49%	5.3%
650	3.81	2477	97	51%	20.2	2.57	88%	67%	50%	0.9%
650	4.62	3003	122	54%	19.8	3.25	89%	70%	54%	0.6%
650	5.39	3504	147	58%	17.7	3.89	91%	72%	60%	-1.4%
650	6.00	3900	172	63%	16.0	4.49	92%	75%	65%	-1.6%

In general, Table 2 shows that the HiVHAc EDU2 performs well in keeping the beam collimated, which is expected when operating at high discharge voltage. Less expected is how well collimated the beam is for conditions with lower discharge voltages. This may be partly attributed to the fact that the boron nitride channels are fresh at the time of testing. The plume divergence may increase as the downstream corners of the channel walls become more chamfered from erosion. Faraday probe testing with chamfered channel walls is planned for a future test.

V. Limitations of Radial Sweep

Although we obtained useful data for determining whether the plasma plume changed from the vibration testing, the ion current density measurements described in this paper also revealed several limitations inherent in radially-swept Faraday probe that are not present for polarly-swept Faraday probe.

By far the biggest limitation associated with sweeping Faraday probe radially is the difficulty in determining the proper integration limits. Generally, radially-swept results are more sensitive to the effects of non-beam ions, background noise, and systematic offset than polarly-swept results. This is because unlike for radial sweeping, termination limits for polar sweeping are well defined, typically at ±90°, and the probe distance from the thruster is fixed.[5] The effects of non-beam ions are more difficult to characterize for the radial sweep because the changing distance between the probe and the thruster also means a changing influence of charge-exchange effect on the signal. To illustrate the difference in the sensitivity of the analysis to background noise and systematic offset between radial sweeping and polar sweeping, let us insert an additional term into Eqs. (1) and (2) to represent these effects. Equation (9) shows the result of adding the noise/systematic offset term into Eq. (1), the charge-weighted divergence angle for polar sweeping.

$$< \cos\delta >_j \approx \frac{2\pi R^2 \int_0^{\pi/2} \left(j(\theta)\cos\theta\sin\theta + N\right) d\theta}{2\pi R^2 \int_0^{\pi/2} \left(j(\theta)\sin\theta + N\right) d\theta} = \frac{2\pi R^2 \left(\frac{\pi}{2} N + \int_0^{\pi/2} j(\theta)\cos\theta\sin\theta\, d\theta\right)}{2\pi R^2 \left(\frac{\pi}{2} N + \int_0^{\pi/2} j(\theta)\sin\theta\, d\theta\right)} \tag{9}$$

In this equation, N is a noise/systematic offset term and is independent of the angle θ. Regardless of spectral characteristics of N, as long as the magnitude is much less than the integral term, the measurement will be largely unaffected by N. Equation (10) shows the result of adding the noise/systematic offset term into Eq. (2), the charge-weighted divergence angle for radial sweeping.

$$< \cos\delta >_j \approx \frac{2\pi \int_0^L \left(j_z(r)\cos\theta + N\right) r dr}{2\pi \int_0^L \left(j_z(r) + N\right) r dr} = \frac{2\pi \left(\frac{L^2 N}{2} + \int_0^L j_z(r)\cos\theta\, r dr\right)}{2\pi \left(\frac{L^2 N}{2} + \int_0^L j_z(r)\, r dr\right)}, \cos\theta = \frac{z_p}{\sqrt{r^2 + z_p^2}} \tag{10}$$

In this equation, N is independent of the radial position r. Unlike Eq. (2), the upper integration limit has been replaced with a finite limit L. For Eq. (10), in the limit that L goes to infinity, the result becomes dominated by the noise/systematic offset term. As that happens, if N is mostly positive, Eq. (10) will asymptotically approach 1 and the δ approach 0°. If N is mostly negative, Eq. (10) will first approach 0, become increasingly negative, becomes singular, then asymptotically approach 1 from positive infinity. If N is randomly distributed, like a typical noise source, the result can exhibit either type of behavior for any given trace. Thus, when analyzing radially-swept Faraday probe data, the integration limit L must be chosen to minimize the influence of noise and offsets while still capturing the bulk of the beam ions. Since the analysis for radially-swept Faraday probe is more sensitive to noise, it is important to use a well-calibrated, well-shielded measurement circuit and electrical lines.

Another important limitation of radially-swept Faraday probe in the current implementation is that the probe is generally not facing the thruster. The probe collection area seen by the thruster when the probe is off to the side of the chamber is distinctly different than when it is on the thruster centerline. This will turn out to make analysis of the effective collection area difficult and is the reason why the probe area correction factor proposed in Brown's dissertation work[5] could not be applied.

VI. Probe Design Lessons Learned

Prior to the two current density tests described in this paper, another Faraday probe test was carried out with an older GRC Faraday probe design. Figure 11 shows the cross section of this older probe design. During this test, which took place concurrently with the performance acceptance test of the HiVHAc EDU2, erratic behavior in the recorded probe signal was found. Specifically, the signal amplitude would undergo large step-wise jumps. Post test analysis showed that a large amount of conductive deposits had accumulated at the bottom of the gap between the collector and guard ring despite there not being a line-of-sight from the plasma to the interior of the gap. Figure 12 shows a picture of the ceramic insulator after the aforementioned test. The location of this deposit is pointed out in Fig. 11. We hypothesize that for some of the higher power operating conditions, enough of the plasma may be able to directly or indirectly strike the interior of the gap. The sputtered molybdenum (the material of the collector and guard ring) is re-deposited on the ceramic insulator, forming an erratic short.

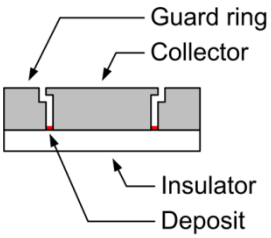

Figure 11. Older Faraday probe cross section. *Region where deposition was found is pointed out.*

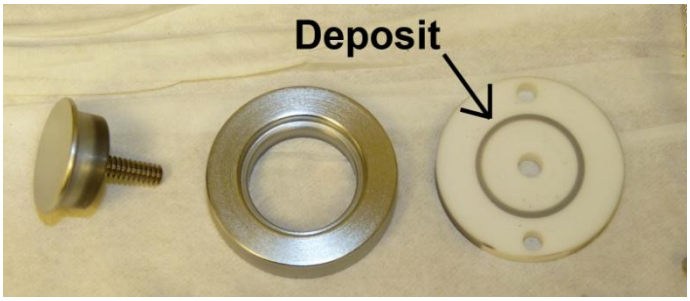

Figure 12. Older Faraday probe disassembled after a test.

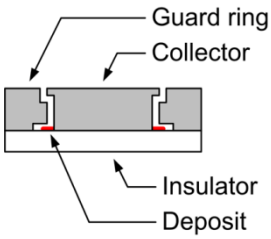

Figure 13. Modified Faraday probe cross section. *Region where deposition was found is pointed out.*

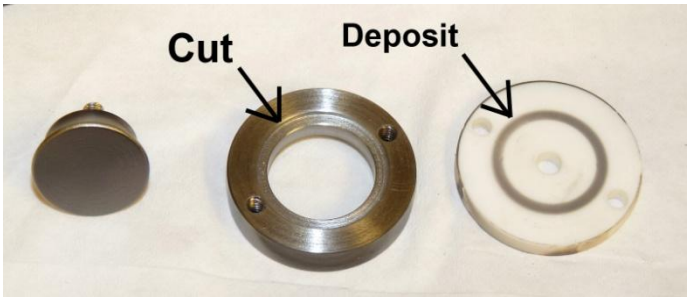

Figure 14. Modified Faraday probe disassembled after a test.

To counter this problem, modification in the form of a simple cut to the guard ring was made to the Faraday probe design. This cut greatly increased the distance over which conductive deposit would have to build up in order to short the guard ring to the collector. Figure 13 shows a cross section of the re-designed Faraday probe with the location of the deposit indicated. This is the design used for the pre-vibration and post-vibration ion current density tests. Figure 14 shows the disassembled modified-probe after testing. Caliper measurement showed that the outer diameter of the deposit is 1.5 mm less than the inner diameter of the guard ring. The modification successfully removed the issue of deposits in the gap shorting the collector and guard ring.

VII. Conclusion and Future Work

Several conclusions were reached in the course of performing the work described in this paper. The original objective of the test was to determine whether the plasma plume of the HiVHAc EDU2 is changed by vibration testing. While some discrepancies are found in the center of the ion current density profiles, these are believed to be artifacts of how the plasma is coupling to the chamber. Since these discrepancies make little contribution to the divergence of the thruster, it is concluded that the plume underwent no meaningful change. The plume divergence angle of the thruster was found to vary from 16° to 28° with higher discharge voltage conditions having lower divergence angle.

In the course of performing the described work, it was discovered that 4-e threshold-based integration limits work fairly well when analyzing radially-swept Faraday probe data. Further analysis performed using the 5-factor phenomenological efficiency model showed that the plume divergence efficiency of the HiVHAc EDU2 varied from 80 to 90% over the discharge voltage range of 200 to 650 V. The analysis also showed that the current utilization varied from 50 to 85%. Using approximate formulas for the other three factors in the 5-factor model, the reconstructed anode efficiency matches fairly well with the anode efficiency derived only from thrust.

Uncertainty analysis on radial sweeping versus polar sweeping reveals that radial sweeping is much more sensitive to noise and systematic offsets. In addition, analysis of the effective collection area is made more difficult when the Faraday probe is not always facing the thruster.

Although the original goal of the ion current density tests are met, it is recommended that future testing revert back to polar sweeping as opposed to radial sweeping. Future work includes repeating the ion current density test with a polarly-swept setup while keeping all else equal. Analysis of polarly-swept data will improve our understanding of what integration limits work well for radially-swept data. Additional future work will also be performed to determine if any further improvements (on top of what is described in this paper) can be made to the

Faraday probe design and the measurement methodology in preparation for the HiVHAc EDU2 long duration wear test.

Acknowledgments

We thank the NASA Science Mission Directorate In-Space Propulsion Technology project for funding this work and Todd Peterson for managing the HiVHAc project. We also thank Thomas Haag for valuable contributions to this work.

References

[1]Dankanich, J. W., Kamhawi, H., and Mathers, A. J., "HiVHAC Maximum Operating Power Mission Impacts", *31st International Electric Propulsion Conference*, 2009-213, Ann Arbor, MI, 20-24 Sep., 2009.

[2]Kamhawi, H., "In-Space Propulsion High Voltage Hall Accelerator Development Project Overview", *47th AIAA/ASME/SAE/ASEE Joint Propulsion Conference & Exhibit*, AIAA-2011-5520, San Diego, CA, 31 Jul.- 3 Aug., 2011.

[3]Kamhawi, H., et al., "NASA's High Voltage Hall Accelerator Engineering Development Unit Performance and Environmental Tests Summary", *48th AIAA/ASME/SAE/ASEE Joint Propulsion Conference & Exhibit*, Atlanta, GA, 29 Jul.- 1 Aug., 2012.

[4]Brown, D. L. and Gallimore, A. D., "Evaluation of ion collection area in Faraday probes", *Review of Scientific Instruments*, Vol. 81, No. 6, doi:10.1063/1.3449541, 25 Jun., 2010, pp. 063504.

[5]Brown, D. L., "Investigation of Flow Discharge Voltage Hall Thruster Characteristics and Evaluation of Loss Mechanisms", Ph.D. Dissertation, Aerospace Engineering, University of Michigan, Ann Arbor, MI, 2009.

[6]Soulas, G. C., Foster, J. E., and Patterson, M. J., "Performance of Titanium Optics on a NASA 30 cm Ion Thruster", *36th AIAA/ASME/SAE/ASEE Joint Propulsion Conference*, AIAA-2000-3814, Huntsville, AL, 16-19 Jul., 2000.

[7]Soulas, G. C., Domonkos, M. T., and Patterson, M. J., "Performance Evaluation of the NEXT Ion Engine", *39th AIAA/ASME/SAE/ASEE Joint Propulsion Conference & Exhibit*, AIAA-2003-5278, Huntsville, AL, 20-23 Jul., 2003.

[8]Pollard, J. E., Diamant, K. D., Crofton, M. W., Patterson, M. J., and Soulas, G. C., "Spatially-Resolved Beam Current and Charge-State Distributions for the NEXT Ion Engine", *46th AIAA/ASME/SAE/ASEE Joint Propulsion Conference & Exhibit*, AIAA-2010-6779, Nashville, TN, 25-28 Jul., 2010.

[9]Hofer, R. R., et al., "Efficacy of Electron Mobility Models in Hybrid-PIC Hall Thruster Simulations", *44th AIAA/ASME/SAE/ASEE Joint Propulsion Conference & Exhibit*, AIAA-2008-4924, Hartford, CT, 21-23 Jul., 2008.

[10]Reid, B. M., "The Influence of Neutral Flow Rate in the Operation of Hall Thrusters", Ph.D. Dissertation, Aerospace Engineering, University of Michigan, Ann Arbor, MI, 2008.

[11]Reid, B. M., Shastry, R., Gallimore, A. D., and Hofer, R. R., "Angularly-Resolved ExB Probe Spectra in the Plume of a 6-kW Hall Thruster", *44th AIAA/ASME/SAE/ASEE Joint Propulsion Conference & Exhibit*, AIAA-2008-5287, Hartford, CT, 21-23 Jul., 2008.